Development of 3D-Printed Composite Running Blades for Pediatric Lower-Limb Prostheses

O. Packham[1], J.S. Schofield[2], Q. Sanders[3,4], and G. W. Melenka[1*],

[1] Mechanical Engineering, York University, Toronto, Ontario, [2] Mechanical and Aerospace Engineering, UC Davis, Davis, U.S.A, [3] Department of Bioengineering and [4]Department of Mechanical Engineering, George Mason University, Fairfax, VA, U.S.A

* *Garrett W. Melenka (gmelenka@yorku.ca)*

Keywords: *3D Printing; Composite Materials; Continuous Fibre 3D printing; Biomechanics; Continuous fibre reinforcement technology*

1. Abstract

Due to the different biomechanics at play, children with lower-limb amputations are prescribed different prostheses for daily use and running. Running-specific prostheses (RSPs) are better suited for physical activities and require an appropriate level of stiffness to return sufficient energy during running while remaining lightweight, which has led many to use composite materials in their manufacturing. Using traditional composite material layup techniques, manufacturing an RSP to meet the needs of specific patients requires a bespoke mold and a hand-layup process, which significantly increases manufacturing costs and limits customization. Basic lower-limb prostheses are often extremely expensive, and, on average, have a replacement interval of three years in Canada, making RSPs prohibitively expensive for families with growing children. To address these issues, new manufacturing methods should be explored to reduce these barriers. Markforged 3D printers utilize continuous fibre reinforcement technology (CFRT) to produce highly customizable composite parts quickly and affordably. For reinforcement layers, CFRT uses concentric fibre reinforcement surrounded by a matrix shell. Most of the volume of a CRFT part is infill, which is treated as a plastic/void composite equal to the infill percentage. Reinforcement layers are also sandwiched between solid floor and ceiling layers, which themselves are treated as a plastic/void composite to account for the gaps between rasters. CFRT-based composite blades may be a promising approach for improving the manufacturing and accessibility of RSPs; however, RSPs fabricated using this approach have yet to undergo systematic mechanical validation to confirm optimal fibre placement, orientation, and composite layup patterns under dynamic loading. Moreover, for this application, characterization is needed to identify the relationship between patient biomechanics (weight, stride length, and running speed) and the mechanical properties of CFRT required to achieve the desired stiffness for an RSP. The aims of this work are to fabricate an optimized RSP with a controlled fibre architecture, quantify the mechanical stresses these blades experience during use, and establish a predictive model linking patient weight and gait characteristics to the required stiffness of the prosthesis. In this work, specifically, a classical laminate plate theory (CLPT) MATLAB code is used to predict the mechanical properties of CFRT test components as well as test RSPs manufactured to ASTM

1. Introduction

Children with lower-limb trans-tibial amputations require different prostheses for daily use and running. Running-specific prostheses (RSPs) require an appropriate stiffness to return sufficient energy during running while remaining lightweight. RSPs are often made from composite materials, such as carbon or glass fibres embedded in a polymer matrix, which provide reinforcement, increasing strength and stiffness without drastically increasing weight. However, conventional composite manufacturing techniques and the unique needs of each patient make them unaffordable for many users. The average cost of a basic lower-limb prosthesis is at least $10,000 CAD [1], and it has a 3-year replacement interval in Canada [2]. However, children outgrow prosthesis devices rapidly due to physical development, necessitating more frequent replacement. Clinical guidelines suggest that children under the age of five may require a new prosthesis annually, while those between the ages of five and twelve typically require replacement every two years [3], leaving low-income families with young children a choice between covering the cost of a new prosthesis out of pocket or using old, incorrectly sized prostheses for multiple years as the child grows out of them. In 2024, 4.7% of new amputees enrolled in the War Amps program were children[4]. An estimated 1.4% of children globally live with amputations[5], which highlights the scale of this problem both nationally and globally. Children without prostheses report experiencing social stigma or exclusion, and the inability to participate in sports and recreational activities [5]. Without a proper prosthesis, running can be uncomfortable or even impossible, which dissuades children from engaging with their peers in physical activities and is an important stage in their development.

RSPs are a type of special prosthesis designed to accommodate/support the biomechanical demands during running. Unlike standard walking prostheses, RSPs are engineered specifically for high-impact, dynamic activities and are optimized to store and return elastic energy throughout the gait cycle. Typically constructed from advanced composite materials such as carbon fibre, these prostheses have a curved, blade-like geometry that allows them to deform under load during the stance phase and then release that stored energy to aid in forward propulsion during toe-off. Traditional manufacturing methods use multiple layers of polyester resin-impregnated fibre sheets formed over a wooden or metal mold to achieve the desired curve and thickness. Varying the rotation of each layer can change the strength and stiffness of the RSP.

A systematic review by Rahnama et al. highlights that the majority of modern RSPs are manufactured from carbon fibre composites due to their high strength-to-weight ratio and ability to efficiently store and return elastic energy during the stance phase of running. These devices function mechanically as curved leaf springs, in which, under deformation, ground reaction forces enable energy storage, followed by energy return during toe-off. This process is highly dependent on material stiffness, hysteresis, and structural design[6]. According to Rahnama et al., one of the most popular, commercially available RSPs had a reported stiffness of 38.7 MPa (Flex Foot Cheetah, Össur, Reykjavík, Iceland) [6] while custom RSPs manufactured and characterized by Abood et al., reinforced with glass fibre and carbon fibre, had a reported stiffness of 28 MPa and 57 MPa, respectively [7]

Using composite material traditional layup techniques, manufacturing an RSP to fit the needs of specific patients requires a bespoke mould and hand-layup process. Traditional composite manufacturing significantly increases costs and limits customization. Typically, the fibre orientation, matrix and lamina materials, and the thickness of the composite layup are the main factors affecting the stiffness and strength of a laminate. The degree of customizability, however, is hindered by this: in woven textiles, the fibre angle is constant for each lamina and cannot be changed locally. This is not a problem for CFRT, however, as it enables non-universal reinforcement, allowing dynamic stiffness across the geometry of a composite part.

Continuous Fibre Reinforcement Technology (CFRT) is a method of additive manufacturing like fused filament fabrication additive manufacturing with the addition of isotropic or concentric fibre reinforcement on specified layers. Unlike continuous fibre technology printers (CFT) that add fibre reinforcement to every filament raster of a 3D printed by embedding the reinforcement material in the filament extrudate during extrusion, CFRT printers have a second nozzle for adding fibre reinforcement, which allows it to only reinforce selected layers[8]. In addition to only reinforcing select layers, CFRT allows for different reinforcement approaches, primarily isotropic and concentric reinforcement. The isotropic reinforcement approach allows for solid layers (no infill) of primarily reinforcement filament printed in the same direction. The printer can be instructed to print each subsequent reinforced layer with a different raster direction to emulate adjusting the fibre orientation on subsequent lamina in a traditional composite layup. The concentric reinforcement approach allows for loops of reinforcement to be added between the shell wall loops and the infill inside the part. The primary benefit of concentric reinforcement is weight reduction and material savings due to the presence of infill. CFRT can produce parts with properties comparable to those of traditional composite layups. By varying the fibre volume fraction (the percentage of fibre content to matrix content) of a part, the stiffness and strength can be carefully tuned. Many variables can affect the fibre volume fraction and, by extension, the stiffness, including the location of the reinforcement groups, the number of reinforcement loops per layer, and the reinforcement material. However, the degree to which this has been studied is minimal.

This study is therefore focused on characterizing the flexural modulus of glass fibre-reinforced samples produced using CFRT. The flexural modulus is a critical mechanical property that reflects a material's resistance to bending deformation and is particularly relevant for load-bearing biomedical devices such as RSPs.

2. Methodology

2.1. Standards and Test Geometry

Using Autodesk Fusion, a simple part geometry was made according to ASTM D790, following the recommended dimensions for molded plastic sample. Since there are no recommended dimensions for 3D-printed samples, the dimensions were used due to the similarity in material choices (thermoplastic polymers). The dimensions also allow for more room to accommodate increased reinforcement in the samples. Figure 1 a) and b) show the typical reinforcement regime of a concentrically reinforced CFRT part from the side and top views. Figure 1 c) shows the standard dimensions of an ASTM D790 molded plastic test sample used in this study.

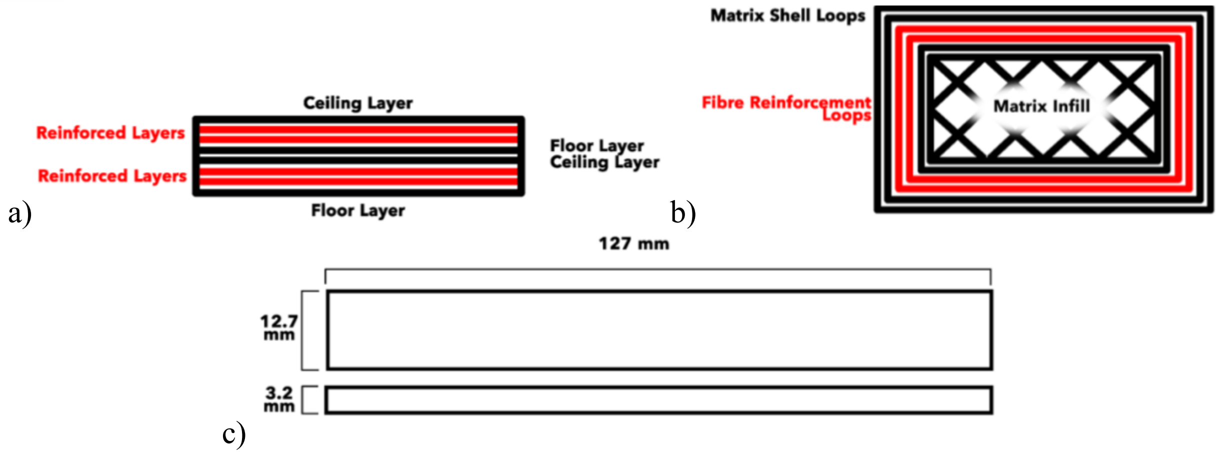

Figure 1: a) Continuous Concentric Fibre Reinforcement Side View, b) Continuous Concentric Fibre Reinforcement Top View, c) Test sample dimensions according to ASTM D790

The sample was prepared using 3D printer slicing software (Eiger 1.2, MarkForged, Somerville, MA), which converts CAD geometries into layered manufacturing instructions and allows detailed control over fibre reinforcement strategies. Eiger.io allows for continuous fibre reinforcement of selected layers. For these samples, a CFRT 3D printer (Onyx Pro, MarkForged, Somerville, MA) was used, which allows for glass fibre reinforcement. The number of loops directly determines the local fibre density and thus significantly influences the stiffness and strength of the sample, as increasing the number of rings increases the proportion of load carried by the high-strength continuous fibres. In the context of CFRT printing, the fibre volume fraction represents the ratio of the deposited continuous fibre material to the total material (matrix plus fibre) used in the part.

For this study, one goal was to achieve the maximum fibre volume fraction in a part while maintaining the key aspects of CFRT components to understand the upper limit of concentric reinforcement. A final fibre volume fraction of 33.52% was achieved for the glass fibre-reinforced samples. A different CFRT 3D printer (Mark 2 Pro, MarkForged, Somerville, MA), which allows a wider range of reinforcement materials, was used to produce a sample reinforced with carbon fibre using the same reinforcement scheme. Interestingly, due to the glass fibre reinforcement filament having a smaller diameter than the carbon fibre reinforcement filament, the fibre volume fraction of the carbon fibre sample was significantly less at 25.12% than that of the glass fibre-reinforced sample. Since the filament diameter of the carbon fibre reinforcement is larger, Eiger.io requires carbon fibre-reinforced parts to be printed at a higher layer height (0.125 mm vs 0.1 mm), resulting in fewer reinforced layers per group. Figure 2 shows the reinforcement regime used for producing the glass fibre-reinforced samples. The top of the image shows the vertical cross-section of the sample, where the white lines represent the infill printed in the matrix filament, and the yellow area is the reinforced geometry of the selected reinforcement group. The bottom of the image shows the five groups of reinforced layers from left to right.

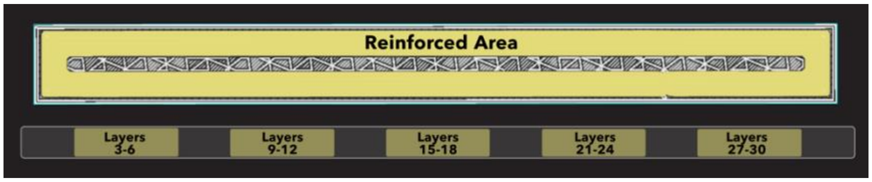

Figure 2: Reinforced D790 Standard Geometry

The reinforcement regimes for both the carbon fibre and glass fibre-reinforced samples are described in Table 1. Due to the different diameters of the reinforcement materials, the samples were printed with different layer heights, meaning that the glass fibre-reinforced samples had a greater number of reinforced layers and therefore a higher fibre volume fraction.

Table 1: Sample Reinforcement Regimes

	Reinforced Layers	Reinforcement Loops/Layer	Number of Reinforced Layers	Fibre Volume Fraction	Layer Height (mm)
Glass Fibre	3-6, 9-12, 15-18, 21-24, 27-30	5	20	33.52%	0.125
Carbon Fibre	3-5, 8-10, 13-14, 17-19, 22-24	5	14	25.12%	0.1

The samples were printed according to the reinforcement regimes described in Table 1 for the specified reinforcement material. Otherwise, the printing parameters were identical for the two sample types. The general printing parameters used are described in Table 2.

Table 2: General 3D Printing Parameters

Infill Percentage	37%
Infill Type	Triangular Fill
Infill Direction	37.5
Floor and Ceiling Layers	4
Wall Loops	2
Wall Thickness	0.2 mm

ASTM D790 recommends a minimum of five tests to ensure accurate results and to account for any errors that may occur during testing. Since this study primarily focuses on the performance of glass fibre-reinforced samples, only a single carbon fibre-reinforced sample was tested for comparison. Future studies will focus on a proper testing regime for both glass fibre- and carbon fibre-reinforced samples.

2.2. Direct Image Correlation (DIC)

Direct Image Correlation (DIC) is a non-contact optical measurement technique widely used in experimental mechanics to quantify full-field displacements and strains on a specimen surface. The method relies on applying (or utilizing) a stochastic speckle pattern on the specimen surface and tracking the motion of these patterns between a reference image and a sequence of images taken during testing. By correlating pixel subsets between images, DIC algorithms can determine displacement fields with subpixel resolution, enabling highly detailed strain mapping across the entire area of interest.

In a typical application, DIC is used to measure deformation directly on the specimen surface; however, in this study, the technique was instead applied to track the displacement of the central loading nose in a three-point bending setup. This was done to improve the accuracy of the displacement measurements. Conventional testing systems, such as the one used for this study (Electropuls E3000, Instron Engineering Corporation, Norwood, MA), often infer displacement from actuator movement, which can introduce systematic error due to compliance within the load frame and load cell. Such compliance leads to discrepancies between the recorded machine displacement and the actual deformation experienced by the specimen. Previous studies have demonstrated that DIC can serve as a "virtual extensometer," directly measuring displacements between points of interest and providing results that are comparable to or more reliable than those from traditional contact-based measurement devices.

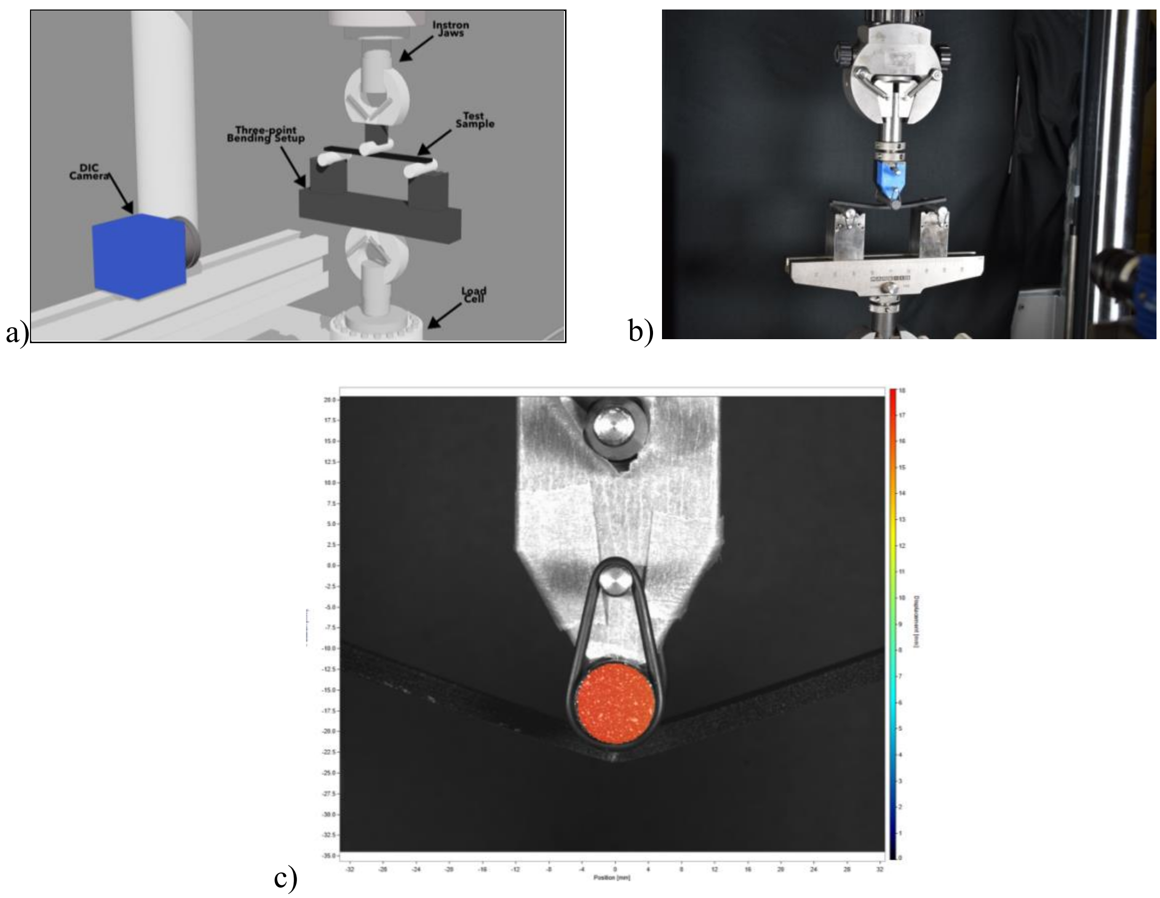

Figure 3: a) DIC Arrangement b) A sample in the Instron E3000 UTM c) DIC Analysis of the Flexural Testing of a Carbon Fibre-Reinforced Sample

Figure 3 a) and b) shows the DIC setup used for the testing. The sample is held between the jaws of the three-point bending setup, with a camera (M-lite 5M, LaVision, Göttingen, Germany) with a 50mm lens placed 489 millimetres from the sample, recording at 10 frames per second. This distance was chosen because it ensures the sample and loading nose remained in focus and in the frame throughout the test. Figure 3 shows the output from the DIC image processing software (DaVis 10.2.1 StrainMaster, LaVision, Göttingen, Germany). Tracking the displacement of the loading nose improves measurement accuracy, as the chosen test frame doesn't account for compliance within the load cell, leading to displacement measurement inaccuracy.

2.3. Numerical Solution

Using a modified form of classical laminate plate theory (CLPT) and a volume-averaged stiffness approach [8], a numerical solution is used to estimate the stiffness of simple (box-shaped) CFRT parts, taking into account the effect of the distinct sections that make up a CFRT part (shell, floor and ceiling layers, infill, concentric reinforcement) as well as the void content between rasters. By estimating the volume fraction and stiffness of each section for the appropriate material, the part's effective flexural modulus can be calculated. The code for this solution is written in MATLAB (MATLAB_R2025a, The MathWorks, Inc., Natick, MA) and is currently still a work in progress.

3. Results

A total of 6 tests were performed: 5 glass fibre-reinforced samples and 1 carbon fibre-reinforced sample. None of the glass fibre-reinforced samples fractured under load. While it's likely that the samples would have fractured over time, their ends collided with the supports of the three-point bending setup, which provided additional support and resistance to fracture. Future tests will use thinner supports to prevent this. Using image processing software (DaVis 10.2.1 StrainMaster, LaVision, Göttingen, Germany), the DIC videos were analyzed to determine the precise displacement of the loading noses, while the load cell data were analyzed in MATLAB.

4. Discussion

The displacement (in millimetres) of the central loading nose was tracked using DIC and analyzed against the applied load (in Newtons) for each sample. Figure 4 shows the analysis of loading nose displacement in the DIC software (DaVis 10.2.1 StrainMaster, LaVision, Göttingen, Germany) of the carbon fibre-reinforced sample. Load–displacement curves obtained from such tests typically exhibit an initial linear region corresponding to elastic behaviour, followed by a nonlinear region associated with damage initiation and propagation within the composite structure.

The results of the load-displacement curves are shown in Figure 4. From the figure, one can see that for all the glass fibre-reinforced samples, the displacement of the loading nose begins to plateau after approximately 10 millimetres without fracturing, unlike the carbon fibre-reinforced sample, which reached its yield point after approximately 12.6 millimetres and 146.9 Newtons. As explained earlier, this plateau is the time at which the samples first contacted the supports of the loading noses. The load-displacement curve can be used to determine the tangent modulus of elasticity for the samples by measuring the slope of the linear region for each and using Equation 1 where the length of the sample between the loading supports, L, is equal to 100 millimetres, the sample width, b, is equal to 12.7 millimetres, the sample depth, d, is equal to 3.2 mm, while the slope of the load-displacement curve, m, is calculated for each test from the results.

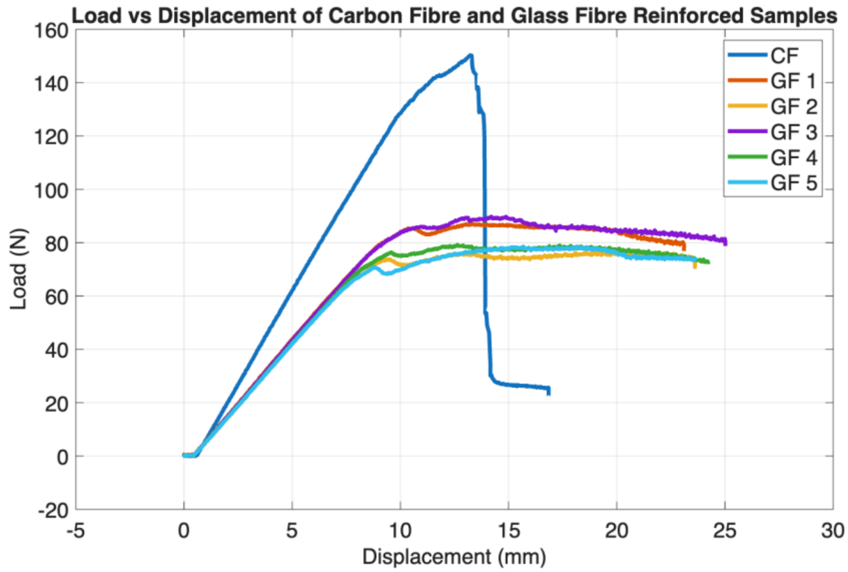

Figure 4: Load vs Displacement of Carbon Fibre and Glass Fibre Reinforced 3D Printed Samples

$$E_f = \frac{L^3 m}{4bd^3} \quad (1)$$

The tangent modulus of elasticity represents the instantaneous stiffness of a part in the elastic region. Table 3 shows the measured slope, sample dimensions and modulus of elasticity for each sample.

Table 3: Tangent Modulus of Elasticity of Carbon Fibre and Glass Fibre Reinforced 3D Printed Samples

Sample	E_f (GPa)
CF	8.172
GF (Average)	5.44 ± 0.11

From Table 3, the carbon fibre-reinforced sample had a much higher tangent modulus of elasticity compared to the glass fibre-reinforced samples. None of the glass fibre-reinforced samples fractured during flexural testing but instead exhibited noticeable plastic deformation, indicating that the material did not undergo catastrophic failure within the tested load range. This behaviour is characteristic of glass fibre-reinforced polymer composites, which typically exhibit higher strain-to-failure and more progressive damage mechanisms than stiffer, more brittle fibre systems. Figure 5 compares the tangent modulus of elasticity for the single carbon fibre-reinforced sample that was tested with the average value of glass fibre-reinforced samples, as well as the values calculated using the numerical solution.

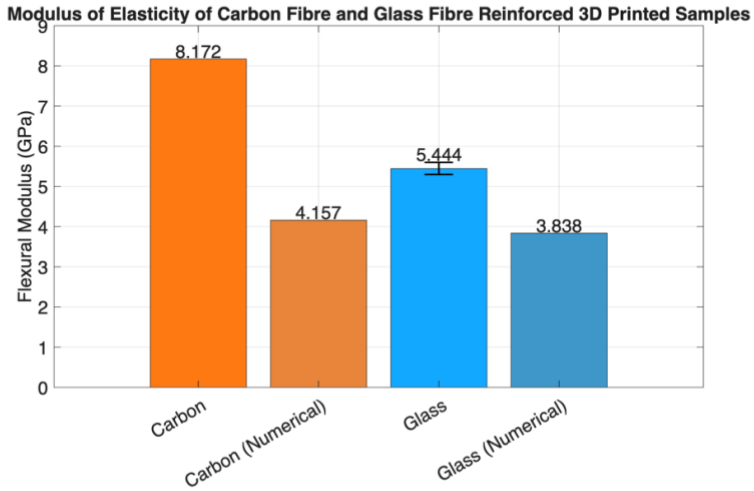

Figure 5: Modulus of Elasticity of Carbon Fibre and Glass Fibre Reinforced 3D Printed Samples

From the figure, the numerical solution for the tangential modulus of elasticity for both the carbon fibre and glass fibre-reinforced samples severely underestimates the experimental solution and needs further refinement. It can also be seen that even with a reduced fibre volume fraction (74.9% lower), the carbon fibre-reinforced sample exhibited a much greater (50.2% increased) tangential modulus of elasticity compared to the glass-fibre reinforced samples. This highlights the importance of reinforcement material selection for the desired use of the CFRT 3D printed component. While the carbon fibre-reinforced samples exhibit a higher instantaneous stiffness, the compliance of RSPs may benefit from the pseudo-ductile response of the glass fibre-reinforced samples. Further research is underway to determine the effect of continuous fibre reinforcement in 3D-printed composite RSPs and the influence of different fibre volume fractions on the tangential modulus of elasticity. These high stiffness values indicate that CRFT is more than capable of manufacturing parts that meet or exceed the requirements for an RSP, compared with the stiffness values reported in the systematic review by Rahnama et al. The largest stiffness value reported by Abood et al. is far less than that achieved with either reinforcement material.

5. Conclusions

This study examined the flexural testing of a 3D-printed ASTM D790 sample with continuous glass fibre and carbon fibre reinforcement produced using a CFRT 3D printer (Mark 2 Pro, MarkForged, Somerville, MA). The reinforcement material had an apparent impact on the flexural modulus of elasticity of the samples, with the carbon fibre-reinforced sample exhibiting an instantaneous stiffness of 8.172 GPa at fraction, and the glass fibre-reinforced samples exhibiting an average instantaneous stiffness of 5.444 GPa during plastic deformation, which is far greater than the stiffness of traditionally manufactured carbon fibre and glass fibre-reinforced RSPs at 28 MPa and 57 MPa, respectively. These results highlight the ability of CFRT 3D printing to offer greater customizability than traditionally manufactured composite components. Future work is focused on the characterization of RSPs, both commercial devices and 3D printed, using similar material testing methods, as well as further flexural testing of similar samples with varying fibre volume fractions to determine their impact on the flexural stiffness and an improved numerical solution to hopefully facilitate the development of a method of predicting the performance of CFRT FFF 3D printed components.

6. References

[1] J. Southards, "Amputee Blade Runners (ABR)." [Online]. Available: https://fillauer.com/2023/10/26/amputee-blade-runners-abr/

[2] C. W. Howard, D. K. Saraswat, G. McLeod, A. Yeung, D. Jeong, and J. Lam, "Canada's prosthetic coverage: A review of provincial prosthetic policy," 2019, *Canadian Online Publication Group*. doi: 10.33137/cpoj.v2i2.33489.

[3] D. G. . Smith, J. W. . Michael, and J. H. . Bowker, *Atlas of amputations and limb deficiencies : surgical, prosthetic, and rehabilitation principles*. American Academy of Orthopaedic Surgeons, 2004.

[4] T. War Amps, "2024 Annual Report Improving the quality of life for Canadian amputees ii The War Amputations of Canada • Annual Report 2024," 2024.

[5] T. Al-Okaliy, H. Obeidat, H. Al-Oran, and N. M. Abdel Razeq, "From playgrounds to rehabilitation centers: A qualitative study of the lived experience of children with an amputation," *J. Pediatr. Nurs.*, vol. 85, pp. 223–231, Nov. 2025, doi: 10.1016/j.pedn.2025.07.037.

[6] L. Rahnama, K. Soulis, and M. D. Geil, "A review of evidence on mechanical properties of running specific prostheses and their relationship with running performance," 2024, *Frontiers Media SA*. doi: 10.3389/fresc.2024.1402114.

[7] S. H. Abood and M. H. Faidh-Allah, "Analysis of Prosthetic Running Blade of Limb Using Different Composite Materials," *Journal of Engineering*, vol. 25, no. 12, pp. 15–25, Dec. 2019, doi: 10.31026/j.eng.2019.12.02.

[8] G. W. Melenka, B. K. O. Cheung, J. S. Schofield, M. R. Dawson, and J. P. Carey, "Evaluation and prediction of the tensile properties of continuous fiber-reinforced 3D printed structures," *Compos. Struct.*, vol. 153, pp. 866–875, Oct. 2016, doi: 10.1016/j.compstruct.2016.07.018.